CRYSTAL GROWTH & DESIGN

Article

pubs.acs.org/crystal

Solvothermal Synthesis, Development, and Performance of $LiFePO_4$ Nanostructures

Jianxin Zhu,[†] Joseph Fiore,[‡] Dongsheng Li,[§] Nichola M. Kinsinger,[‡] Qianqian Wang,[‡] Elaine DiMasi,[⊥] Juchen Guo,[†,‡] and David Kisailus*[,†,‡]

[†]Materials Science and Engineering Program, University of California—Riverside, Riverside, California 92521, United States

[‡]Department of Chemical and Environmental Engineering, University of California—Riverside, Riverside, California 92521, United States

[§]Molecular Foundry, Lawrence Berkeley National Laboratory, Berkeley, California 94720, United States

[⊥]Synchrotron Light Source Department, Brookhaven National Laboratory, Upton, New York 11973, United States

Supporting Information

ABSTRACT: We report the synthesis and nanostructural development of polycrystalline and single crystalline $LiFePO_4$ (LFP) nanostructures using a solvothermal media (i.e., water–tri(ethylene glycol) mixture). Crystal phase and growth behavior were monitored by powder and synchrotron X-ray diffraction, as well as transmission electron microscopy (TEM), while particle morphologies were examined using scanning electron microscopy (SEM). Initially, thin (100 nm) platelets of $Fe_3(PO_4)_2 \cdot 8H_2O$ (vivianite, VTE) formed at short reaction times followed by the nucleation of LFP (20 nm particles) on the metastable VTE surfaces. Upon decrease in pH, primary LFP nanocrystals subsequently aggregated into polycrystalline diamond-like particles via an oriented attachment (OA). With increasing reaction time, the solution pH further decreased, leading to a dissolution–recrystallization process (i.e., Ostwald ripening, OR) of the oriented polycrystalline LFP particles to yield evenly sized, single crystalline $LiFePO_4$. Samples prepared at short reaction durations demonstrated a larger discharge capacity at higher rates compared with the single crystalline particles. This is due to the small size of the primary crystallites within larger secondary $LiFePO_4$ particles, which reduced the lithium ion diffusion path while subsequently maintaining a high tap density. Understanding the relationship between solution conditions and nanostructural development as well as performance revealed by this study will help to develop synthetic guidelines to enable efficient lithium ion battery performance.

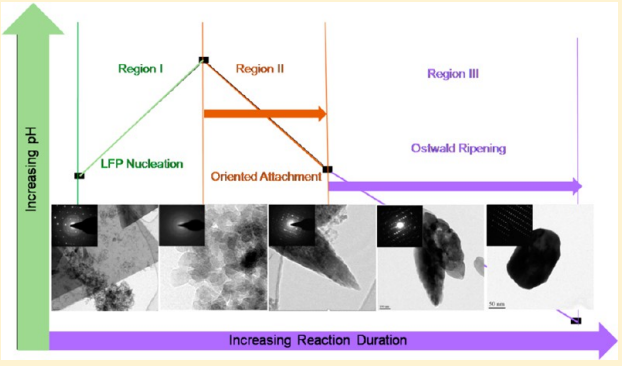

1. INTRODUCTION

As fossil fuel supplies are depleted, efforts to create new and renewable energy sources are being implemented. In addition to the need for renewable energy conversion technologies, there is an urgency for enhanced energy storage for municipal energy storage, electric vehicles, and portable devices. Rechargeable lithium ion batteries offer an effective media to store energy. There has been a marked improvement in Li-ion technologies compared with other alternatives such as the NiCd (nickel–cadmium) or NiMH (nickel–metal hydride) cells. Li-ion cells offer double the specific energy and over three times the energy density versus Ni–H_2 systems (which use pressurized hydrogen), while providing higher energy efficiency.[1]

Improvement in the material components of Li-ion batteries, specifically the cathode and anode, offers potential to enhance their performance. One such cathode, the olivine-structured lithium iron phosphate ($LiFePO_4$, LFP) was invented and reported by Goodenough et al. more than 15 years ago.[2] Because of its low cost, low toxicity, thermal and chemical stability, and good cycle stability, it is an excellent candidate as a cathode in rechargeable lithium batteries used in electric vehicles.[2] However, it is hindered by a low rate capacity due to the poor electronic conductivity and low lithium ion diffusivity, which inhibits expanding its commercial potential.[3,4] In order to overcome this inherent deficiency of LFP, research strategies have focused on utilizing conductive agents (carbon, silver, etc.)[5−7] to increase the electronic conductivity and to improve the mobility of lithium ions via cationic doping.[8,9]

A number of different synthesis methods have been developed to produce controlled LFP including solid phase synthesis,[10,11] sol–gel process,[12] solution coprecipitation,[13] and solvothermal treatments.[14] Solvothermal syntheses, which often operate under higher pressures, offer the potential to precisely

Received: January 13, 2013
Revised: October 6, 2013
Published: October 9, 2013

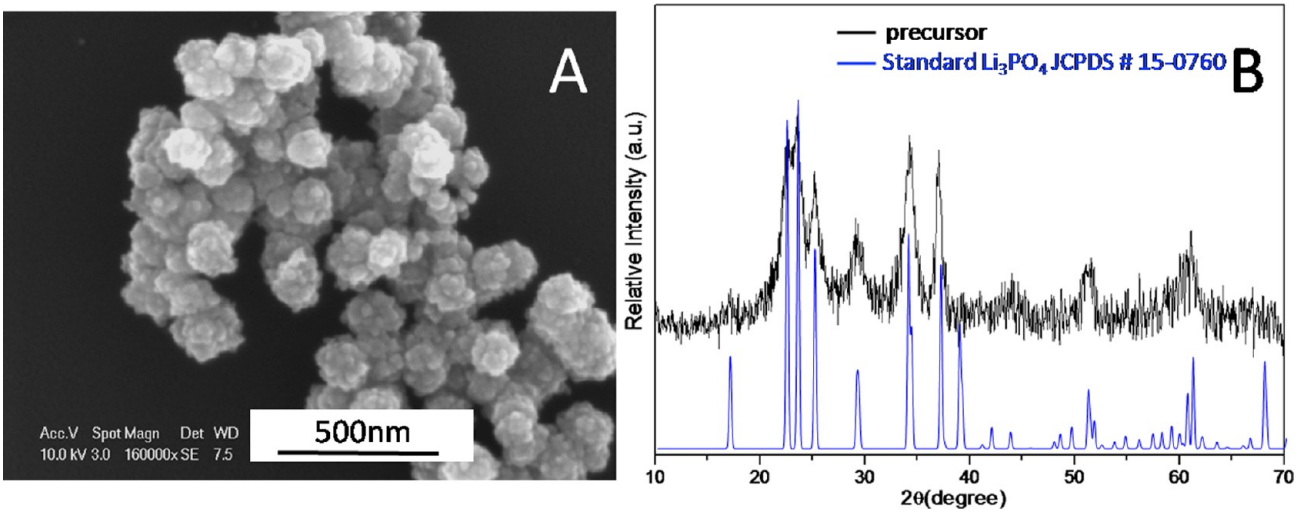

Figure 1. (A) SEM micrograph and (B) XRD pattern of precursor sample indicating the formation of Li_3PO_4 nanocrystals.

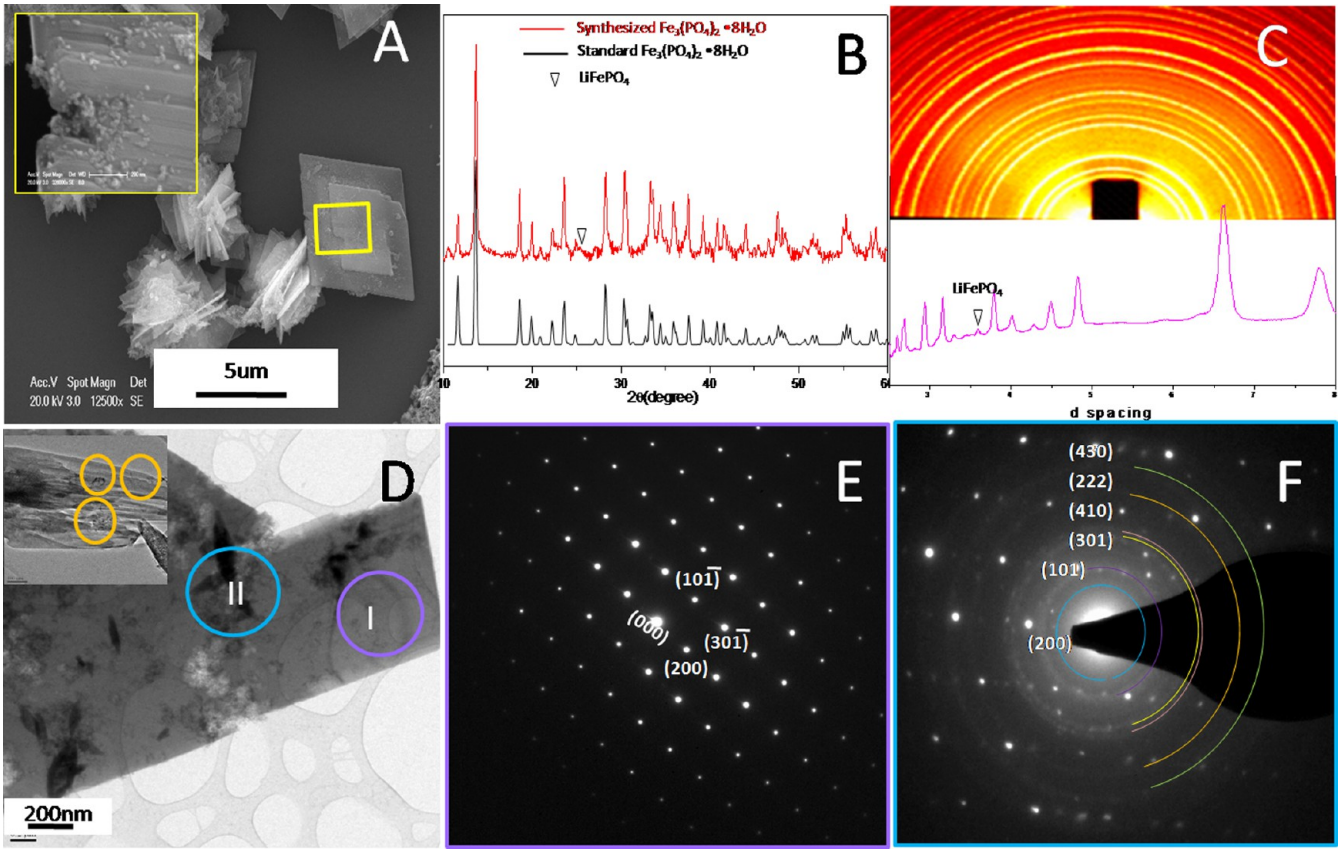

Figure 2. Characterization of the sample synthesized at 160 °C for 5 min. (A) SEM of the platelet structure, (B) powder XRD of sample with $Fe_3(PO_4)_2 \cdot 8H_2O$ as a reference, (C) synchrotron X-ray diffraction of the sample, (D) bright-field TEM of the platelet structure with small particles on top (upper left inset), highlighting LFP nanoparticles forming at edges of $Fe_3(PO_4)_2 \cdot 8H_2O$), (E) SAED from region I (circled purple area), and (F) SAED from region II (circled blue area).

control the size, shape distribution, and crystallinity of particles at low to moderate temperatures.[14−20] Solvents used in the syntheses of LFP have included benzyl alcohol,[14] tetraethylene glycol (TEG),[15] poly(ethylene glycol) (PEG),[16−19] and triethylene glycol.[20] Here, we modify the solution environment by utilizing a mixture of water and triethylene glycol as the solvent to synthesize lithium iron phosphate. Recently Lu et al.[21] reported the hydrothermal mechanism of the LFP formation. However, limited information has been presented to understand the formation mechanism and the resulting crystallinity on the performance in the water-triethylene glycol system. Previous research has revealed the primary lithium-ion insertion pathways in LFP.[22] Thus, by uncovering the formation mechanism of LFP nanostructures and determining the relationship between the resulting structures and function,

dx.doi.org/10.1021/cg4013312 | *Cryst. Growth Des.* 2013, 13, 4659−4666

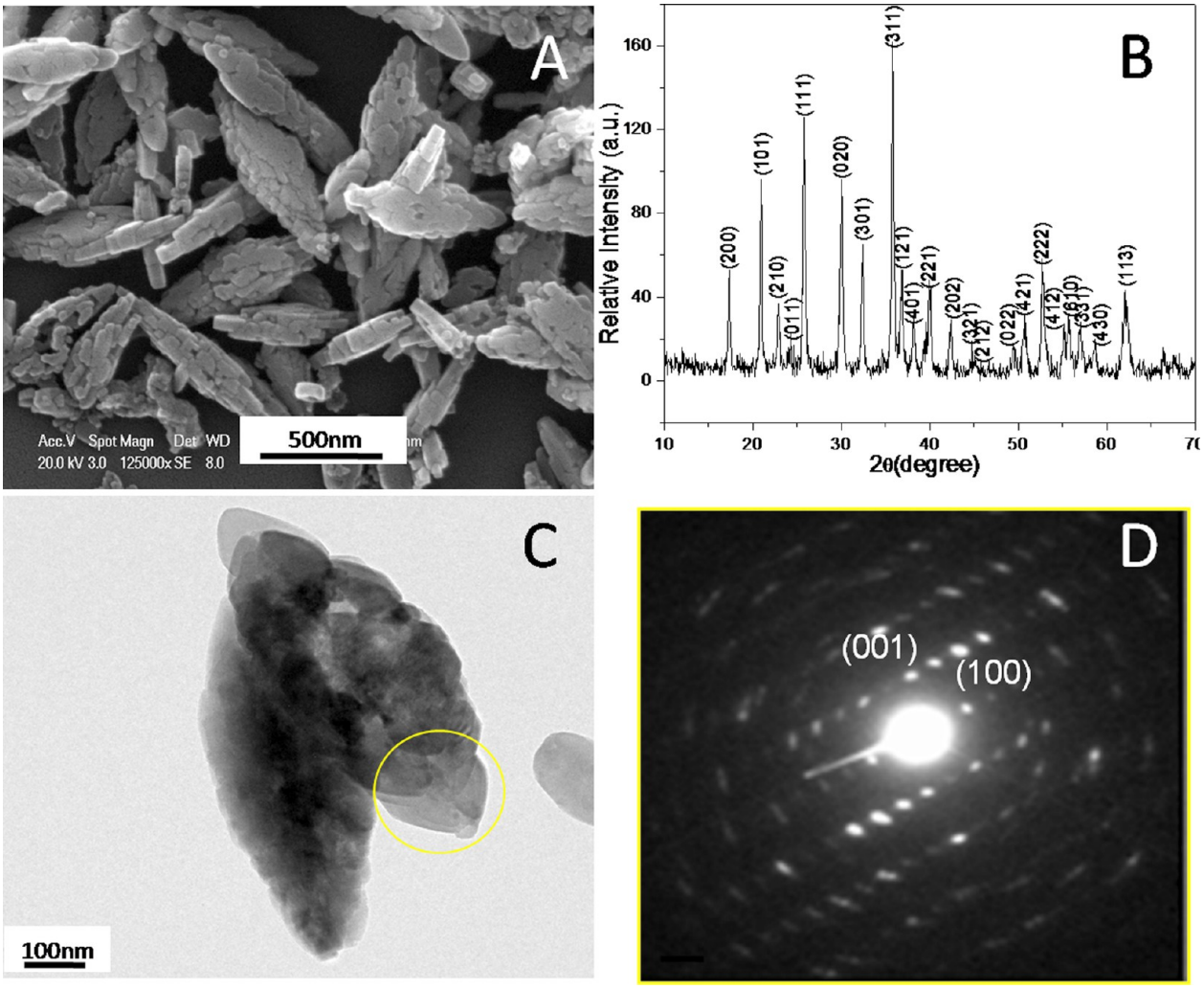

Figure 3. Analyses of $LiFePO_4$ synthesized at 160 °C for 10 min: (A) SEM micrograph highlighting the assembled secondary particles of LFP; (B) powder XRD of sample; (C) bright field TEM with corresponding (D) SAED from the yellow-circled area.

there is a great potential to yield highly efficient, long cycle life Li-ion batteries.

2. EXPERIMENTAL SECTION

2.1. Synthesis of Lithium Iron Phosphate. LFP nanopowders were prepared using a solvothermal method. Stoichiometric amounts of $FeSO_4{\cdot}7H_2O$, H_3PO_4 (85 wt % solution), and $LiOH{\cdot}H_2O$ with a molar ratio of 1:1:3 were used. Briefly, separate aqueous-based ferrous sulfate and lithium hydroxide solutions were made by dissolving $FeSO_4{\cdot}7H_2O$ and $LiOH{\cdot}H_2O$ in degassed Milli-Q water, respectively. After addition of the lithium hydroxide solution into tri(ethylene glycol), aqueous solutions of H_3PO_4 and ferrous sulfate were subsequently added to achieve a homogeneous 0.1 M Fe solution. After vigorous magnetic stirring at room temperature for 10 min, a green suspension formed and was transferred into either glass vials (for short time studies) or Teflon-lined stainless steel autoclaves (for extended reaction durations). Reactors were sealed and heated to 160 °C for 5−900 min. After ambient cooling to room temperature, products were centrifuged, washed several times with deionized water and absolute alcohol, and finally dried in vacuum for 5 h.

2.2. Material Characterization. Phase identification was determined by X-ray diffraction analysis (XRD, Philips X'Pert) using Cu Kα radiation. Using the resulting XRD diffraction patterns, we calculated crystallite diameters based on the Scherer formula.[23] Particle sizes and morphologies were observed using a scanning electron microscope (SEM, FEI XL30) at 10−20 kV accelerating voltage. A transmission electron microscope (TEM, FEI CM300), operated at 300 kV, was used to identify crystallite size, morphology, and phase. Synchrotron X-ray diffraction was performed at beamline X6B of the National Synchrotron Light Source (NSLS) in Brookhaven National Laboratory using 19 keV X-rays and a beam spot focused to 100 μm × 100 μm.

2.3. Electrochemical Performance. As-synthesized $LiFePO_4$ powder, conductive carbon black (Super P), and poly(vinylidene fluoride) (PVDF, 70:20:10 wt %) were mixed in *N*-methylpyrrolidone (NMP) to produce a slurry. This viscous slurry was subsequently coated on an aluminum foil current collector. The coated film was dried in the vacuum oven at 100 °C for 12 h. Coin cells (R2032 type) were assembled in an argon-filled glovebox, consisting of the prepared positive electrode, lithium metal foil as the negative electrode, Celgard polymer as a separator, and 1.0 M $LiPF_6$ in ethylene carbonate (EC)−diethyl carbonate (DEC) (50:50 vol %) as the electrolyte solution. The loading of the active material was 1.5 mg/cm^2. The cyclic performance and rate capability of $LiFePO_4$ batteries were tested using an Arbin battery test system (Arbin Instruments, model BT2043). Cyclic voltammograms were run on a VMP3 multichannel electrochemical station.

3. RESULTS AND DISCUSSION

3.1. Formation and Nanostructural Evolution of $LiFePO_4$. *3.1.1. Precursor.* Precursor particles, which formed after 10 min of stirring, were collected via centrifugation,

dx.doi.org/10.1021/cg4013312 | *Cryst. Growth Des.* 2013, 13, 4659−4666

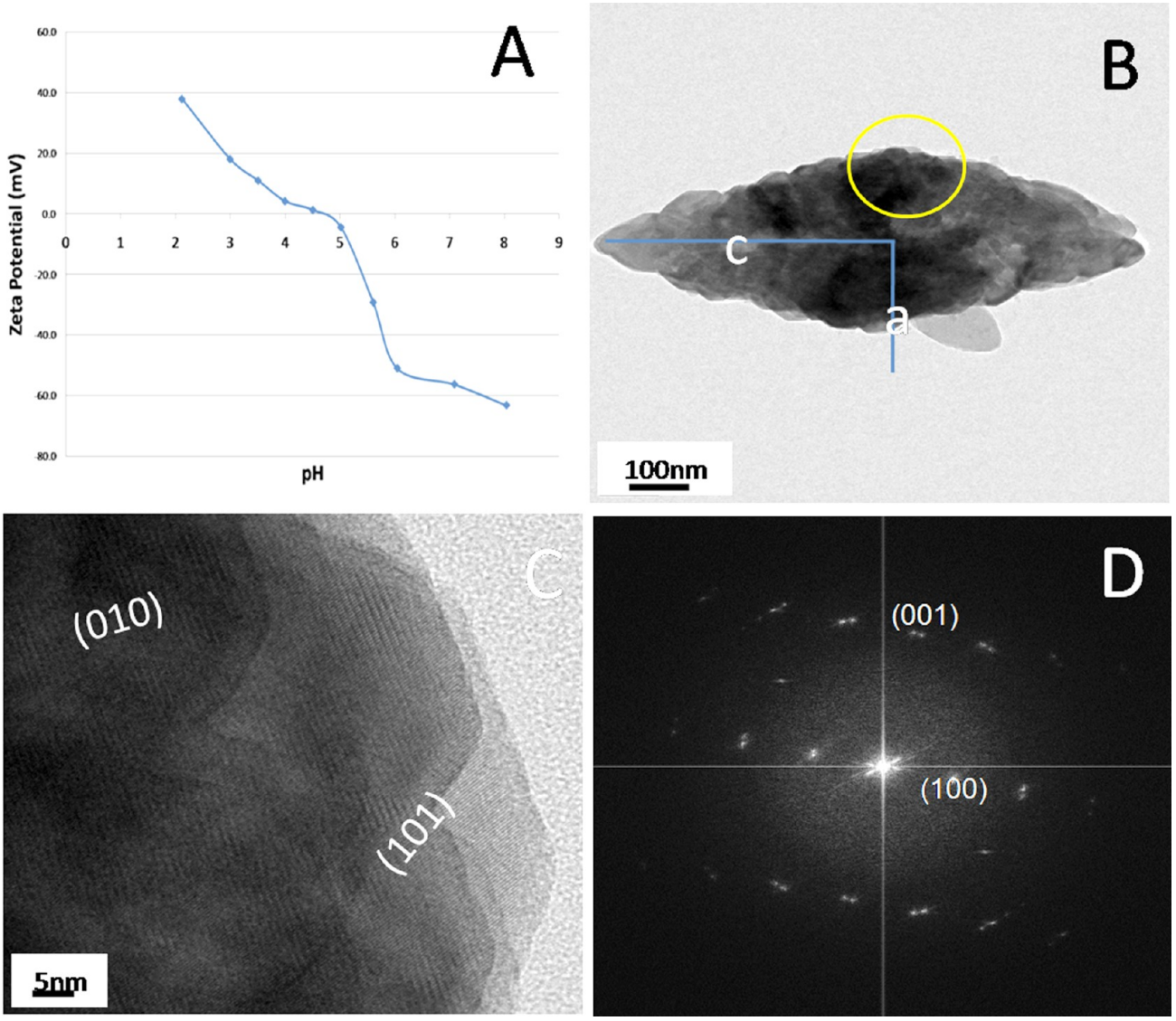

Figure 4. Characterization of $LiFePO_4$ synthesized at 160 °C for 10 min: (A) ζ potential analysis of LFP particles; (B) bright field TEM showing *c* and *a* directions of particles; (C) HRTEM from yellow circle highlighted in panel B and (D) the corresponding FFT.

washed (as described in section 2.1), and dried in a vacuum oven. SEM (Figure 1A) demonstrates the aggregated nature of the nanoparticles, and XRD (Figure 1B) revealed that these nanoparticulate precursor powders consist of ∼10 nm (as calculated by Scherer equation[23]) crystallites of Li_3PO_4 (JCPDS No. 15-0760).

3.1.2. Formation of $Fe_3(PO_4)_2{\cdot}8H_2O$ (Vivianite, VTE) and Nucleation of $LiFePO_4$. The precursor-based slurries were subsequently placed in sealed reactors at 160 °C. After a 5 min reaction duration, large plate-like (5 μm × 5 μm × 100 nm thick) nanostructures (Figure 2A) formed with small particles on their surfaces (inset in Figure 2A). Examination of these products by powder XRD (Figure 2B) and synchrotron X-ray analysis (Figure 2C) revealed the formation of crystalline sheets of VTE ($Fe_3(PO_4)_2{\cdot}8H_2O$, JCPDS No. 30-0662), as well as small quantities of $LiFePO_4$. The precursor particles, which consist of Li_3PO_4, dissolve (K_{sp} = 3.2 × 10^{-9}) and in the presence of iron ions yield a less soluble $Fe_3(PO_4)_2{\cdot}8H_2O$ (K_{sp} = 1 × 10^{-36}). In addition, it is noteworthy that the tri(ethylene glycol) solvent serves as a reducing agent, providing a favorable environment for vivianite formation.[24,25]

Interestingly, we observed that small particles appear to form at the edges or kinks on the VTE plates (see insets, Figure 2A,D). Bright field TEM (Figure 2D) and SAED (Figures 2E,F) were used to confirm the phases of both plate-like structures and the small particles on the plate surfaces. The SAED pattern shown in Figure 2E represents the region highlighted in purple (region I). Analysis of this diffraction pattern confirmed the near single crystalline nature of the plates as $Fe_3(PO_4)_2{\cdot}8H_2O$. SAED analysis of region II (highlighted in blue, Figure 2D), which contains small particles on the platelet surface, reveals a combination of the nearly single crystalline $Fe_3(PO_4)_2{\cdot}8H_2O$ and diffraction rings that correspond to $LiFePO_4$ (i.e., the nanoparticles on the surface of the platelets are $LiFePO_4$). Here, it is likely that under the reaction conditions, $Fe_3(PO_4)_2{\cdot}8H_2O$ is dissolving (as observed by striations on platelets, Figure 2A), providing high concentrations of nutrient for the nucleation of $LiFePO_4$.[26]

3.1.3. Oriented Assembly of Polycrystalline $LiFePO_4$ (LFP) Particles. After 10 min reaction duration at 160 °C, only pure phase $LiFePO_4$ was detected via XRD (Figure 3B). All the reflections were indexed as an orthorhombic olivine-type

dx.doi.org/10.1021/cg4013312 | *Cryst. Growth Des.* 2013, 13, 4659−4666

Table 1. Reaction pH at Different Reaction Durations

reaction time (min)	0	5	10	15	20	60	180	900
pH	5.51	6.05	5.54	5.18	4.83	4.60	4.39	4.30

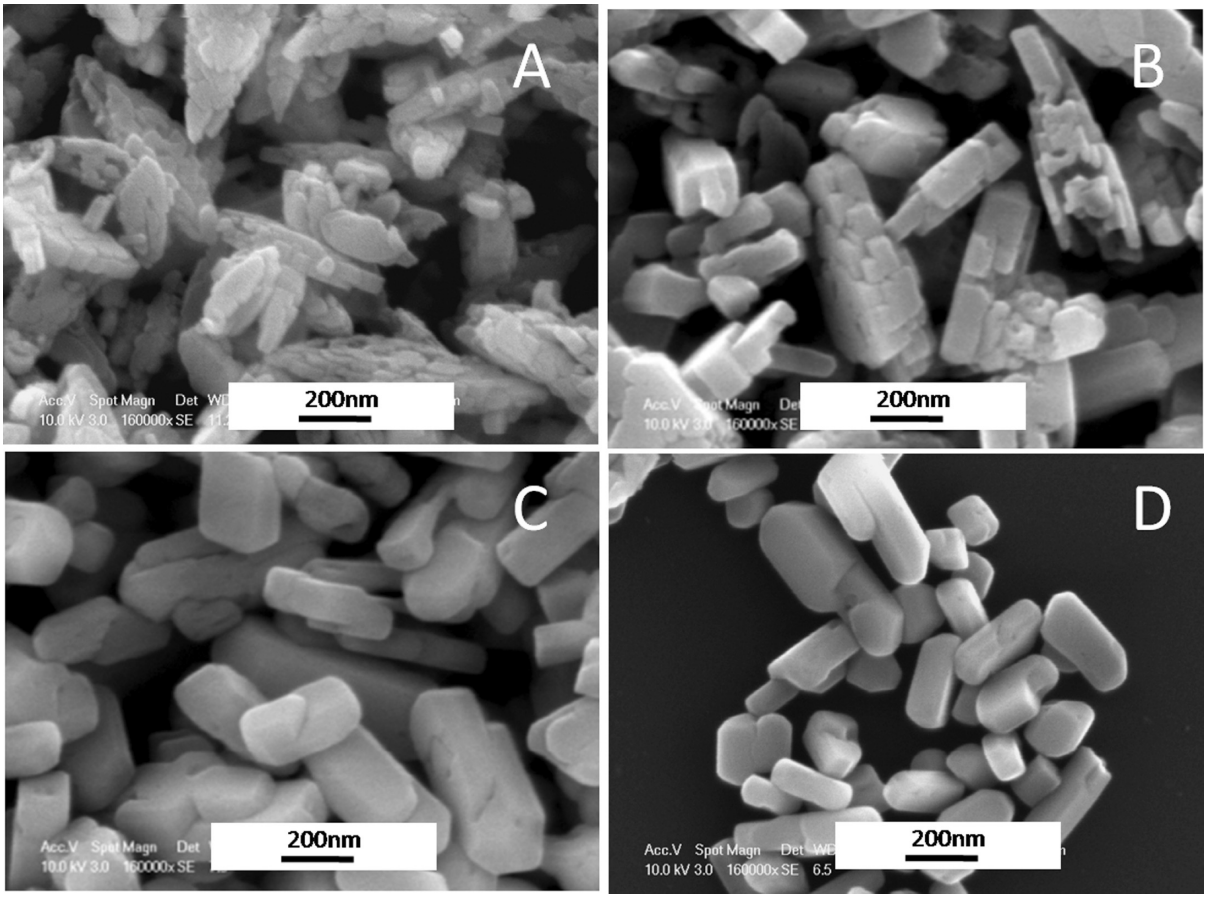

Figure 5. SEM micrographs of LFP products at 160 °C with increasing duration: (A) after 10 min, LFP formation and assembly into secondary particles is completed; increasing reaction duration to (B) 60 min, (C) 420 min, and (D) 900 min yields more crystalline LFP.

structure (JCPDS No. 81-1173), and no additional impurity phases were observed, confirming the removal of vivianite. Rietveld refinement of the XRD data with the *Pnma* space group gave the following lattice parameters: a = 10.334(1) Å, b = 6.010(1) Å, and c = 4.694(1) Å, which are in good agreement with the reported values (a = 10.332(2) Å, b = 6.005(1) Å, c = 4.693(6) Å) that used a high temperature synthesis method.[27] The crystallite size of the LFP was calculated to be 39 nm using the Scherer equation[23] and was confirmed with bright field TEM (data not shown). The particles (Figure 3A) displayed a diamond-like morphology and appeared to be formed by an oriented assembly of primary particles. Bright field TEM (Figure 3C) was conducted to further investigate the nanostructure of these particles. Electron diffraction (Figure 3D) analysis of one of the particles in Figure 3C revealed a pseudo-single-crystal pattern, which consisted of arched (ca. ~5°) diffraction spots. This indicates that the larger, secondary diamond-like particles are likely to consist of an oriented assembly of smaller primary particles.

In order to investigate the potential assembly of primary particles, we interrogated the surface charge of LFP using ζ potential measurements (Figure 4A) to determine their interactions in the reaction suspension. The primary nanoparticles of $LiFePO_4$ initially form at pH ≈ 6 (Table 1). Here, these particles are highly negatively charged (i.e., ζ = −52 mV) and electrostatically repel each other. However, as the reaction duration increases, the pH continually decreases (below 5.5). Subsequently, the charge on the particles becomes less negative (i.e., ζ < −20 mV), which enables particles to approach each other more closely, enabling their assembly.[28,29] At this stage, the primary LFP particles appear to aggregate in an oriented manner, forming larger diamond-like secondary particles.

Further bright field TEM analysis of one of the secondary particles is shown in Figure 4B. High-resolution TEM imaging (Figure 4C) with the corresponding fast Fourier transform (FFT, Figure 4D) of this particle reveals that primary nanoparticles are indeed attached to each other in an oriented manner and are aligned in [001] and [100] directions, with the (010) plane as the primary exposed surface. Ceder et al.[30] have calculated surface energies of the olivine structured $LiFePO_4$ using density functional theory (DFT) within the generalized gradient approximation (GGA) + U framework. Their results show that the low-energy surfaces are in the [100], [010], [011], [101], and [201] directions. Islam et al.[31] reported that the (010) and (100) planes have the lowest attachment energies in their simulation, which corroborates our observations of diamond-like structures elongated in the [001] direction with short [010] lithium diffusion pathways. This

dx.doi.org/10.1021/cg4013312 | *Cryst. Growth Des.* 2013, 13, 4659−4666

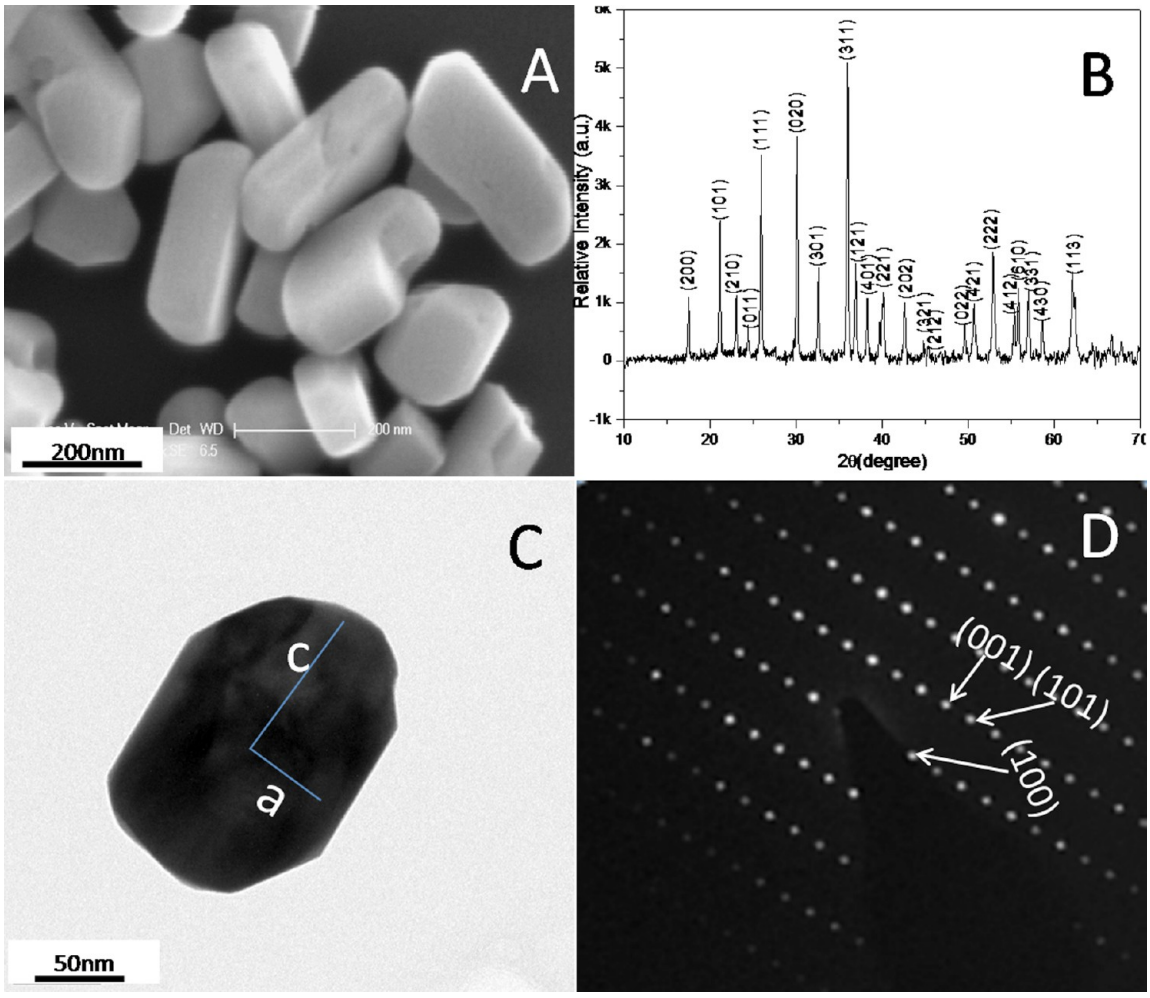

Figure 6. Analysis of single crystalline $LiFePO_4$ synthesized at 160 °C for 900 min. (A) SEM of powder sample highlighting size and morphological features, (B) XRD pattern confirming pure $LiFePO_4$, (C) Bright field TEM micrograph of a $LiFePO_4$ particle, and (D) the corresponding SAED from panel C, confirming its single crystalline nature.

result enables a foundation for modifying experimental conditions to design particles with controlled thickness along the [010] direction (the primary lithium ion diffusion path) and therefore enhance the Li-ion battery performance.

3.1.4. Ostwald Ripening of Polycrystalline LFP. For longer duration reactions, Teflon-lined autoclaves were used with the same synthesis conditions used in the glass tubes. Here, liners were filled with the same volume (43.5 vol %) of precursor suspension in order to provide a similar head space and ensure the overall pressure in the reactors was the same in both glass and Teflon-lined reactors. After filling and sealing the liners, reactors were heated at 160 °C for different durations (60–900 min). Subsequent analyses of products from both reactors under the same reaction conditions confirmed the similarity (particle size, crystallinity, and shape) of products between these two reactions (see Supporting Information, Figure 1S).

SEM micrographs (Figure 5) highlight size and morphology changes of LFP particles at different reaction durations. As the reaction duration increases, the large secondary particles decrease in size with a concurrent increase in crystal size and decrease in number of grain boundaries per particle (Figure 5A–D). For example, the secondary particles are as long as 900 nm (Figure 3) and consist of 39 nm primary crystals (as calculated by the Scherer equation). With increasing reaction durations (i.e., 60 and 420 min in Figures 5, panels B and C, respectively), the crystal size increases to 95 and 280 nm, respectively (as measured from SEM and TEM). At the longest reaction duration (900 min), significantly smaller particles have formed (ca. 450 nm long) but seem to have no internal grains (i.e., single crystalline). Measurement of reaction pH versus time (Table 1) indicates a decrease in pH after 5 min. This decrease in pH is due to net consumption of OH^- groups (see eqs 1 and 2) as more phosphate anions (PO_4^{3-}) and ferrous cations (Fe^{2+}) are consumed during the formation of $LiFePO_4$ (eq 3). The reaction schemes are shown as follows:

$$PO_4^{3-}{}_{(aq)} + 2H_2O_{(l)} \rightleftharpoons H_2PO4^- + 2OH^- \quad (1)$$

$$Fe^{2+} + 6H_2O_{(l)} \rightleftharpoons Fe(H_2O)_5(OH)^+{}_{(aq)} + H^+ \quad (2)$$

$$Li^+ + PO_4^{3-} + Fe^{2+} \rightleftharpoons LiFePO_4 \quad (3)$$

This decrease in pH increases the solubility of $LiFePO_4$ due to acidity and high temperature conditions.[32] This increased solubility enables a dominating dissolution–crystallization (Ostwald ripening, OR) of these particles, with their subsequent densification and formation of more crystalline particles. The morphology also changes from a diamond-like structure at 10 min to polygonal prisms at 900 min, providing evidence for the dominating crystal growth mechanism.[33] The

dx.doi.org/10.1021/cg4013312 | Cryst. Growth Des. 2013, 13, 4659–4666

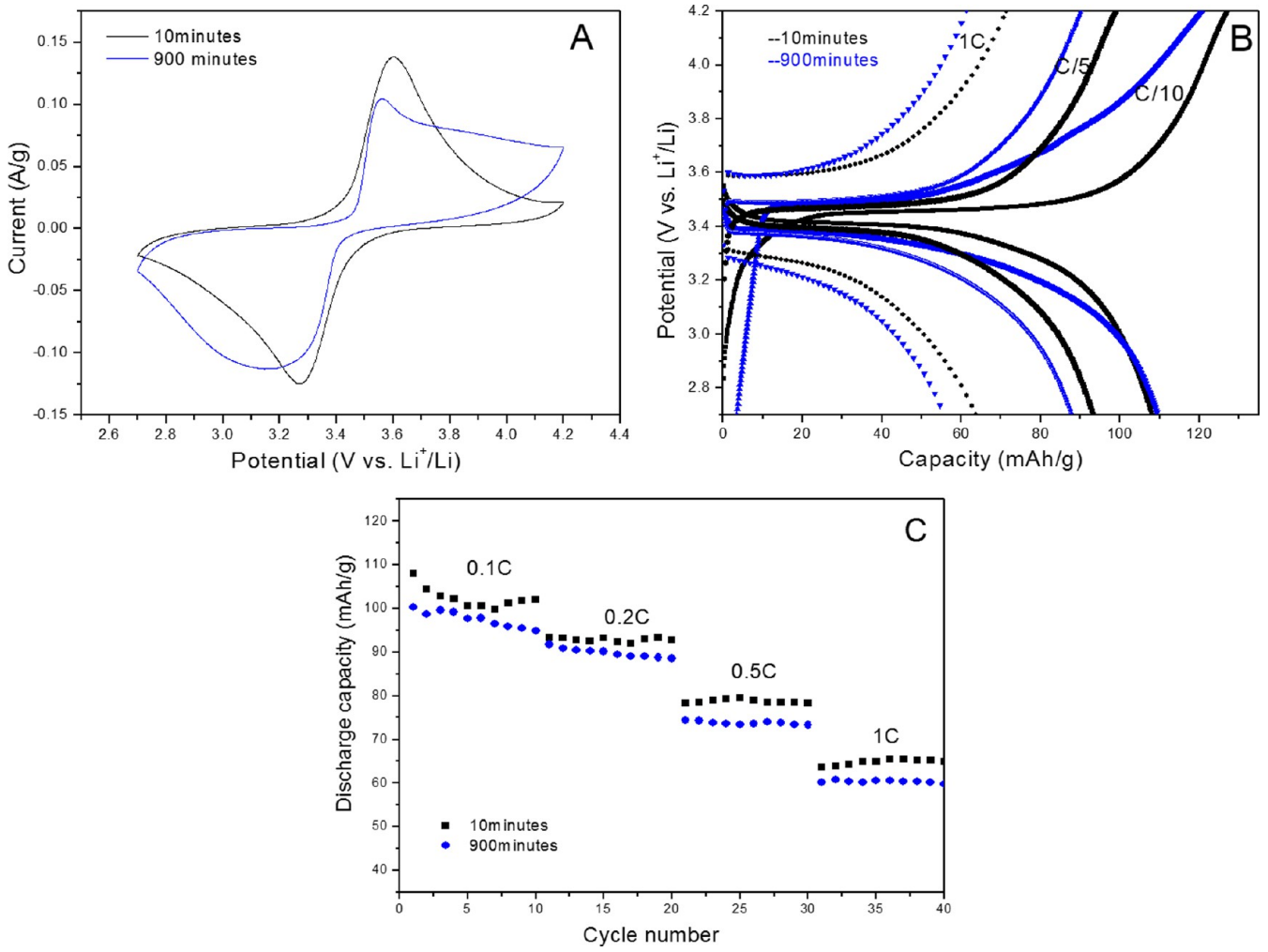

Figure 7. Electrochemical characterization of polycrystalline and single crystalline LFP: (A) CV profiles in the voltage range of 2.7−4.2 V at a scan rate of 0.2 mV/s, (B) galvanostatic charge/discharge profiles, and (C) cycling performance at various current rates between 2.7 and 4.2 V (vs Li^+/Li).

drum-like polygonal $LiFePO_4$ crystals are the equilibrium morphology, which has been shown by both experiment and simulation.[21,31]

3.1.5. Development of Single Crystalline LFP. SEM imaging of the powder products after 900 min at 160 °C (Figure 6A) reveals a nanorod structure. These nanorods were measured (more than 40 particles) to be 450 ± 60 nm long × 128 ± 24 nm wide × 91 ± 13 nm thick. XRD (Figure 6B) confirms the formation of highly crystalline $LiFePO_4$ (indexed as the orthorhombic olivine-type structure, JCPDS No. 81-1173) without any detectable impurity phases. Bright field TEM analysis with SAED (Figures 6C,D) of one particle revealed its single crystalline nature with elongation along the *c* direction and a (010) surface plane.

3.2. Electrochemical Performance. In order to relate LFP structure to performance, electrochemical measurements were conducted for both polycrystalline and single crystalline $LiFePO_4$ materials. Cyclic voltammetry (CV, Figure 7A), which was performed at a scan rate of 0.2 mV/s at room temperature, displays an oxidation peak and reduction peak, corresponding to the charge/discharge reactions of the Fe^{2+}/Fe^{3+} redox couple. The polycrystalline LFP sample (synthesized at 10 min) displayed a voltage hysteresis (ca. 0.28 V) and a higher peak current (0.14 A/g), while the single crystalline LFP specimen (synthesized at 900 min) had a voltage difference of 0.44 V and a peak current of 0.1 A/g). It is known that smaller voltage differences between the charge and discharge as well as higher peak currents indicate better electrode reaction kinetics and thus better rate performance.[34,35] The results demonstrate that the polycrystalline materials with smaller crystallite sizes (<40 nm along the [010] direction) yield enhanced kinetics compared with single crystal particles during the lithiation and delithiation. Cycling charge/discharge and rate profiles of electrodes with carbon-free (i.e., uncoated $LiFePO_4$) polycrystalline and single crystalline LFP (Figures 7B,C) demonstrate similar specific discharge capacities at C/10 (i.e., 109 and 101 mAh/g for polycrystalline or single crystalline LFP, respectively). Our materials show higher discharge capacity compared with the previously reported measurements of carbon-free 50 nm LFP particles, which displayed a discharge capacity as low as 60 mAh/g at a C/10 rate.[16] Furthermore, at high rate capacities, polycrystalline specimens with smaller crystallite diameters yielded better electrode reaction kinetics and thus higher rate performance (Figure 7C). However, neither of these materials have flat voltage plateaus, which is likely due to the absence of an electrically conductive carbon coating. In addition, it is likely that residual moisture, Fe(III) impurities (see Supporting Information, Figure 2S), and less ordered surfaces may be responsible for reduced performance.

dx.doi.org/10.1021/cg4013312 | *Cryst. Growth Des.* 2013, 13, 4659−4666

4. CONCLUSIONS

We have systematically investigated the crystal nucleation and morphological evolution of $LiFePO_4$ in a water−tri(ethylene glycol) system. $LiFePO_4$ first formed on the high energy surfaces of $Fe_3(PO_4)_2{\cdot}8H_2O$ platelets. As these primary particles are formed, the reaction pH decreases, which reduces the surface charge on $LiFePO_4$ primary particles. This reduction in surface charge enables the primary particles to approach each other and attach in an oriented manner to form secondary particles. These diamond-like LFP particles are oriented along the (010) plane and elongated in the high surface energy direction of [001]. As the reaction proceeds, the pH decreases, promoting the further crystallization and densification (Ostwald ripening, OR) of LFP due to the increased solubility of LFP. Electrochemical characterization of carbon-free LFP materials demonstrate a discharge capacity of more than 100 mAh/g. Polycrystalline particles with smaller primary crystallite diameters afforded higher discharge capacity and better kinetics compared with the single crystalline particles. Based on our understanding of the formation mechanism and the structure−performance relationships in $LiFePO_4$ using an environmental friendly synthetic method, we will continue to produce the $LiFePO_4$ with shorter lithium diffusion paths to improve the battery performance.

■ ASSOCIATED CONTENT

Supporting Information

Sample comparison between glass and Teflon-liner reactions and XPS of different reaction duration samples. This material is available free of charge via the Internet at http://pubs.acs.org.

■ AUTHOR INFORMATION

Corresponding Author

*E-mail: david@engr.ucr.edu. Phone: +1-951-827-2260. Fax: +1-951-827-5696.

Notes

The authors declare no competing financial interest.

■ ACKNOWLEDGMENTS

This work is sponsored by Winston Chung Global Energy Center.

■ REFERENCES

(1) Rydh, C. J.; Sandén, B. A. *Energy Convers. Manage.* **2005**, *46* (11−12), 1957−1979.
(2) Padhi, A. K.; Nanjundaswamy, K. S.; Goodenough, J. B. *J. Electrochem. Soc.* **1997**, *144* (4), 1188−1194.
(3) Kim, D.-K.; Park, H.-M.; Jung, S.-J.; Jeong, Y. U.; Lee, J.-H.; Kim, J.-J. *J. Power Sources* **2006**, *159* (1), 237−240.
(4) Gu, Y.-H.; Zeng, C.-S.; Wu, H.-K.; Cui, H.-Z.; Huang, X.-W.; Liu, X.-B.; Wang, C.-L.; Yang, Z.-N.; Liu, H. *Mater. Lett.* **2007**, *61* (25), 4700−4702.
(5) Park, K. S.; Son, J. T.; Chung, H. T.; Kim, S. J.; Lee, C. H.; Kang, K. T.; Kim, H. G. *Solid State Commun.* **2004**, *129* (5), 311−314.
(6) Dominko, R.; Bele, M.; Gaberscek, M.; Remskar, M.; Hanzel, D.; Pejovnik, S.; Jamnik, J. *J. Electrochem. Soc.* **2005**, *152* (3), A607−A610.
(7) Chen, Z. H.; Dahn, J. R. *J. Electrochem. Soc.* **2002**, *149* (9), A1184−A1189.
(8) Yang, M.-R.; Ke, W.-h.; Wu, S.-h. *J. Power Sources* **2007**, *165* (2), 646−650.
(9) Wang, D. Y.; Li, H.; Shi, S. Q.; Huang, X. J.; Chen, L. Q. *Electrochim. Acta* **2005**, *50* (14), 2955−2958.
(10) Liu, H.; Li, C.; Zhang, H. P.; Fu, L. J.; Wu, Y. P.; Wu, H. Q. *J. Power Sources* **2006**, *159* (1), 717−720.
(11) Kang, H.-C.; Jun, D.-K.; Jin, B.; Jin, E. M.; Park, K.-H.; Gu, H.-B.; Kim, K.-W. *J. Power Sources* **2008**, *179* (1), 340−346.
(12) Hsu, K.-F.; Tsay, S.-Y.; Hwang, B.-J. *J. Mater. Chem.* **2004**, *14* (17), 2690−2695.
(13) Lee, M.-H.; Kim, T.-H.; Kim, Y. S.; Song, H.-K. *J. Phys. Chem. C* **2011**, *115* (25), 12255−12259.
(14) Yang, H.; Wu, X.-L.; Cao, M.-H.; Guo, Y.-G. *J. Phys. Chem. C* **2009**, *113* (8), 3345−3351.
(15) Muraliganth, T.; Stroukoff, K. R.; Manthiram, A. *Chem. Mater.* **2010**, *22* (20), 5754−5761.
(16) Yang, S.; Zhou, X.; Zhang, J.; Liu, Z. *J. Mater. Chem.* **2010**, *20* (37), 8086−8091.
(17) Fey, G. T.-K.; Huang, K.-P.; Kao, H.-M.; Li, W.-H. *J. Power Sources* **2011**, *196* (5), 2810−2818.
(18) Wang, L. N.; Zhang, Z. G.; Zhang, K. L. *J. Power Sources* **2007**, *167* (1), 200−205.
(19) Xu, Z.; Xu, L.; Lai, Q.; Ji, X. *Mater. Res. Bull.* **2007**, *42* (5), 883−891.
(20) Lim, J.-S.; Kim, D.-H.; Mathew, V.; Ahn, D.-C.; Kim, J.-K. *J. Nanosci. Nanotechnol.* **2011**, *11* (2), 1451−1454.
(21) Lu, Z.; Chen, H.; Robert, R.; Zhu, B. Y. X.; Deng, J.; Wu, L.; Chung, C. Y.; Grey, C. P. *Chem. Mater.* **2011**, *23* (11), 2848−2859.
(22) Islam, M. S.; Driscoll, D. J.; Fisher, C. A. J.; Slater, P. R. *Chem. Mater.* **2005**, *17* (20), 5085−5092.
(23) Alexander, L.; Klug, H. P. *J. Appl. Phys.* **1950**, *21* (2), 137−142.
(24) Rosenqvist, I. T. *Lithos* **1970**, 3 (4), 327−334.
(25) Fagel, N.; Alleman, L. Y.; Granina, L.; Hatert, F.; Thamo-Bozso, E.; Cloots, R.; André, L. *Global Planet. Change* **2005**, *46* (1−4), 315−336.
(26) Ou, X.; Gu, H.; Wu, Y.; Lu, J.; Zheng, Y. *Electrochim. Acta* **2013**, *96*, 230−236.
(27) Chen, J. J.; Whittingham, M. S. *Electrochem. Commun.* **2006**, *8* (5), 855−858.
(28) Jaffar, S.; Nam, K. T.; Khademhosseini, A.; Xing, J.; Langer, R. S.; Belcher, A. M. *Nano Lett.* **2004**, *4* (8), 1421−1425.
(29) Peng, C.; Thio, Y. S.; Gerhardt, R. A. *Langmuir* **2012**, *28* (1), 84−91.
(30) Wang, L.; Zhou, F.; Meng, Y. S.; Ceder, G. *Phys. Rev. B* **2007**, *76* (16), No. 165435.
(31) Fisher, C. A. J.; Islam, M. S. *J. Mater. Chem.* **2008**, *18* (11), 1209−1215.
(32) Kanamura, K.; Koizumi, S.; Dokko, K. *J. Mater. Sci.* **2008**, *43* (7), 2138−2142.
(33) Finnegan, M. P.; Zhang, H.; Banfield, J. F. *Chem. Mater.* **2008**, *20* (10), 3443−3449.
(34) Lan, Y.; Wang, X.; Zhang, J.; Zhang, J.; Wu, Z.; Zhang, Z. *Powder Technol.* **2011**, *212* (2), 327−331.
(35) Xia, Y.; Zhang, W.; Huang, H.; Gan, Y.; Tian, J.; Tao, X. *J. Power Sources* **2011**, *196* (13), 5651−5658.